In-fiber polarimeters based on hollow-core photonic bandgap fibers

Haifeng Xuan[a], Wei Jin[a]*, Min Zhang[b], Jian Ju[a], Yanbiao Liao[b]

[a]*Department of Electrical Engineering, The Hong Kong Polytechnic University, Hong Kong*
[b]*Department of Electronic Engineering, Tsinghua University, Beijng, China*
*eewjin@polyu.edu.hk

Abstract: In-fiber polarimeters or polarization mode interferometers (PMIs) are fabricated by cascading two CO2-laser-induced in-fiber polarizers along a piece of hollow-core photonic bandgap fiber. Since the two interfering beams are the orthogonal polarizations of the fundamental mode, which are tightly confined to the core and have much lower loss than higher order modes, the PMIs can have either short (e.g., a few millimeters) or long (tens of meters or longer) device length without significantly changing the fringe contrast and hence provide design flexibility for applications required different device lengths. As examples of potential applications, the PMIs have been experimentally demonstrated for wavelength-dependent group birefringence measurement; and for strain, temperature and torsion sensors. The PMI sensors are quite sensitive to strain but relatively insensitive to temperature as compared with fiber Bragg grating sensors. The PMIs function as good directional torsion sensors that can determine the rate and direction of twist at the same time.

OCIS codes: (060.2310) Fiber optics; (060.5295) Photonic crystal fibers; (060.2370) Fiber optic sensors; (230.3990) Microstructure devices.

References and links

1. A. M. Vengsarkar, W. C. Michie, L. Jankovic, B. Culshaw, and R. O. Claus, "Fiber-optic dual-technique sensor for simultaneous measurement of strain and temperature," Lightwave Technology, Journal of **12**, 170-177 (1994).
2. T. Graham, W. Douglas, W. C. Michie, and C. Brian, "In-line mode splitter applied to a dual polarimeter in elliptical core fibre," C. Brian, and D. C. J. Julian, eds. (SPIE, 1994), pp. 339-342.
3. B. K. Kim, S. H. Yun, I. K. Hwang, and B. Y. Kim, "Nonlinear strain response of two-mode fiber-optic interferometer," Opt. Lett. **21**, 934-936 (1996).
4. S. Y. Huang, J. N. Blake, and B. Y. Kim, "Perturbation effects on mode propagation in highly elliptical core two-mode fibers," Lightwave Technology, Journal of **8**, 23-33 (1990).
5. W. Jin, W. C. Michie, G. Thursby, M. Konstantaki, and B. Culshaw, "Simultaneous measurement of strain and temperature: error analysis," Optical Engineering **36**, 598-609 (1997).
6. C. K. kirkendall, and A. Dandridge, "Overview of high performance fibre-optic sensing," Journal of physics. D, Applied physics **37**, 197-216 (2004).
7. E. Udd, *Fiber optic smart structures* (Wiley-Interscience 1995).
8. R. B. Dyott, J. Bello, and V. A. Handerek, "Indium-Coated D-Shaped-Fiber Polarizer," Optics Letters **12**, 287-289 (1987).
9. H. Y. Choi, M. J. Kim, and B. H. Lee, "All-fiber Mach-Zehnder type interferometers formed in photonic crystal fiber," Optics Express **15**, 5711-5720 (2007).
10. L. S. Pieter, "Long-period grating Michelson refractometric sensor," Measurement Science and Technology **15**, 1576-1580 (2004).
11. J. H. Lim, H. S. Jang, K. S. Lee, J. C. Kim, and B. H. Lee, "Mach-Zehnder interferometer formed in a photonic crystal fiber based on a pair of long-period fiber gratings," Opt. Lett. **29**, 346-348 (2004).
12. Y.-J. Kim, U.-C. Paek, and B. H. Lee, "Measurement of refractive-index variation with temperature by use of long-period fiber gratings," Opt. Lett. **27**, 1297-1299 (2002).
13. H. Y. Choi, K. S. Park, and B. H. Lee, "Photonic crystal fiber interferometer composed of a long period f iber grating and one point collapsing of air holes," Opt. Lett. **33**, 812-814 (2008).

#112835 - $15.00 USD Received 15 Jun 2009; revised 11 Jul 2009; accepted 12 Jul 2009; published 17 Jul 2009

14. J. Jian, J. Wei, and H. Hoi Lut, "Compact In-Fiber Interferometer Formed by Long-Period Gratings in Photonic Crystal Fiber," Photonics Technology Letters, IEEE **20**, 1899-1901 (2008).
15. J. Jian, N. M. Li, J. Wei, and H. Hoi Lut, "Photonic bandgap fiber tapers and in-fiber interferometric sensors," Optics Letters (2009).
16. H. F. Xuan, W. Jin, J. Ju, Y. P. Wang, M. Zhang, Y. B. Liao, and M.H.Chen, "Hollow-core photonic bandgap fiber polarizer," Optics Letters **33** (2008).
17. C. M. Smith, N. Venkataraman, M. T. Gallagher, D. Muller, J. A. West, N. F. Borrelli, D. C. Allan, and K. W. Koch, "Low-loss hollow-core silica/air photonic bandgap fibre," Nature **424**, 657-659 (2003).
18. J. C. Knight, "Photonic crystal fibres," Nature **424**, 847-851 (2003).
19. M. Wegmuller, M. Legre, N. Gisin, T. P. Hansen, C. Jakobsen, and J. Broeng, "Experimental investigation of the polarization properties of a hollow core photonic bandgap fiber for 1550 nm," Optics Express **13**, 1457-1467 (2005).
20. G. Bouwmans, F. Luan, J. C. Knight, P. S. J. Russell, L. Farr, B. J. Mangan, and H. Sabert, "Properties of a hollow-core photonic bandgap fiber at 850 nm wavelength," Optics Express **11**, 1613-1620 (2003).
21. Y. P. Wang, W. Jin, J. Ju, H. F. Xuan, H. L. Ho, L. M. Xiao, and D. N. Wang, "Long period gratings in air-core photonic bandgap fibers," Optics Express **16**, 2784-2790 (2008).
22. S. C. Rashleigh, "Measurement of fiber birefringence by wavelength scanning: effect of dispersion," Opt. Lett. **8**, 336-338 (1983).
23. X. Chen, M.-J. Li, N. Venkataraman, M. Gallagher, W. Wood, A. Crowley, J. Carberry, L. Zenteno, and K. Koch, "Highly birefringent hollow-core photonic bandgap fiber," Opt. Express **12**, 3888-3893 (2004).
24. V. Pureur, G. Bouwmans, K. Delplace, Y. Quiquempois, and M. Douay, "Birefringent solid-core photonic bandgap fibers assisted by interstitial air holes," (AIP, 2009), p. 131102.
25. C. Leon, *Time-frequency analysis: theory and applications* (Prentice-Hall, Inc., 1995).
26. O. Frazao, S. O. Silva, J. M. Baptista, J. L. Santos, G. Statkiewicz-Barabach, W. Urbanczyk, and J. Wojcik, "Simultaneous measurement of multiparameters using a Sagnac interferometer with polarization maintaining side-hole fiber," Appl. Opt. **47**, 4841-4848 (2008).
27. B. H. Lee, and J. Nishii, "Self-interference of long-period fibre grating and its application as temperature sensor," (IEE, 1998), pp. 2059-2060.
28. X. Dong, L. Su, P. Shum, Y. Chung, and C. C. Chan, "Wavelength-selective all-fiber filter based on a single long-period fiber grating and a misaligned splicing point," Optics Communications **258**, 159-163 (2006).
29. E. Li, "Temperature compensation of multimode-interference-based fiber devices," Optics Letters **32**, 2064-2066 (2007).
30. Y.-P. Wang, J.-P. Chen, and Y.-J. Rao, "Torsion characteristics of long-period fiber gratings induced by high-frequency CO2 laser pulses," J. Opt. Soc. Am. B **22**, 1167-1172 (2005).
31. L. Chunn-Yenn, A. W. Lon, and C. Gia-Wei, "Corrugated long-period fiber gratings as strain, torsion, and bending sensors," Lightwave Technology, Journal of **19**, 1159-1168 (2001).

1. Introduction

In-fiber interferometers based on the interference of different modes/polarizations have been a subject of continuous interest due to their potential applications as multi-wavelength comb-filters and sensors for multi-parameter measurement[1-5]. As compared with the traditional two-fiber interferometers[6], the in-fiber devices based on a single fiber has the advantage of compactness, common mode noise reduction, and easiness for embedding into materials for smart structure applications[7]. Early works used dual mode elliptical fibers and the interference between the two lowest order LP modes or between different polarizations of the two modes were exploited for simultaneous strain and temperature measurement [1, 3-5]. The mode coupling/splitting for these interferometers was realized by off-set alignments or the use of mode splitters[2]; however, fabrication of the in-fiber devices realizing mode splitting/polarizing is not straightforward and need complex polishing, alignment and/or metal coating procedures[8]. More recently researchers exploited the interference of the fundamental mode with a cladding mode by use of a pair of long period gratings (LPGs) or a combination of a LPG with a non-adiabatic fiber taper or an offset splice [9-14]. These works include in-fiber interferometers in conventional single mode fibers (SMFs) [10, 12] and index-guiding photonic crystal fibers (PCFs)[9, 11, 13, 14], and have been applied for applications such as strain, temperature or refractive index measurement. However, the fringe contrast of these core/cladding mode interferometers decreases quickly with increase of the device length due to the relatively large (and surrounding dependent) loss of the cladding modes, which limit the device to short length.

#112835 - $15.00 USD Received 15 Jun 2009; revised 11 Jul 2009; accepted 12 Jul 2009; published 17 Jul 2009

We have recently demonstrated a core/surface mode in-fiber interferometer in a hollow-core photonic bandgap fiber (HC-PBF) by non-adiabatic tapering of a piece of HC-PBF[15]. The length of such a device is also limited due to the relatively larger loss experienced by the surface mode and the fringe contrast is relatively low because of the small fraction of power coupled into the surface mode.

In this paper, we report a novel in-fiber polarimeter by cascading two in-fiber polarizers made directly on a piece of HC-PBF. The fabrication of such polarizers made by partial collapsing/deforming of air-holes through the use of an automatically scanned pulsed CO_2 laser [16] and the process is straightforward and multiple in-fiber polarizers may be made directly on a single piece of HC-PBF. The two interfering beams are the two orthogonal polarizations of the fundamental mode in a HC-PBF and have much lower transmission losses as compared with cladding/surface modes, even when the fiber is subjected to tight bend[17, 18]. This will allow the development of in-fiber interferometers with basically arbitrary long device length. Unlike the conventional core-cladding interferometers that require the removal of coating of the fiber in the sensing region to avoid significant loss of the cladding modes, coating with basically any refractive index may be applied to the present in-fiber polarimeter without increasing the loss of the two interfering beams. The paper is organized as follows: the basic operating principle and the fabrication of the in-fiber polarimeters are outlined in Section 2, the use of the polarimeter for the measurement of wavelength-dependent group birefringence is described in Section 3, and the responses of the polarimeter to strain, temperature, and twist are presented in Section 4.

2. Operating principle and fabrication of PMI

The HC-PBF PMIs are based on a commercial HC-1550-02 PBF from Crystal-Fiber A/S. The Scanning Electron Microscope (SEM) micrograph of the fiber cross-section is shown in Fig.1(c). The hollow-core has a diameter of ~10.9μm and is surrounded by a holey lattice with an average pitch value of 3.8μm. The holey cladding region has a diameter of 70μm and is surrounded by a ring of solid silica. The total diameter of the fiber is about 120μm. The thickness of the silica bridges between cladding-holes is about 0.34μm, and the air-filling fraction of holey cladding region is above 90%.

As have been shown previously, HC-PBFs have considerable residual birefringence due to the imperfect non-centro-symmetry resulted from the fiber fabrication process [19, 20]. The birefringence existing in the HC-1550-2 PCF results in accumulated phase difference between the two orthogonal polarization modes when they propagate along the PBF, and this is the basis for the stable operation of the in-fiber PMI.

Figure 1(a) is a schematic of a PMI comprising of two in-fiber polarizers fabricated along a commercial HC-1550-02 PBF. Figures 1(b) and 1(d) shows the side view and cross section, respectively, of a typical in-fiber HC-PBF polarizer. The incoming light, which is linearly polarized by the first in-fiber polarizer, excites two orthogonal polarization modes that propagate through physical length *L* along the HC-PBF and recombine at the second polarizer. It should be emphasized that the principal axis of the polarizers are not be along the birefringence axes of the PBF. Assume that the directions of two polarizers are in parallel and are ideally 45°aligned to the birefringence axes of the HC-PBF, the output from the second polarizer may be expressed as

$$I_p = \frac{I_0}{2}(1+\cos(\frac{2\pi}{\lambda}\cdot L\cdot B)) \tag{1}$$

where I_0 is a constant depending on the source light intensity. I_p is PMI output intensity. $B = n_{eff}^x - n_{eff}^y$, n_{eff}^x and n_{eff}^y are respectively the effective refractive index of x- and y-polarization mode. L is the separation between the two polarizations as shown in Fig.1(a), and λ is the wavelength of light in vacuum.

#112835 - $15.00 USD Received 15 Jun 2009; revised 11 Jul 2009; accepted 12 Jul 2009; published 17 Jul 2009

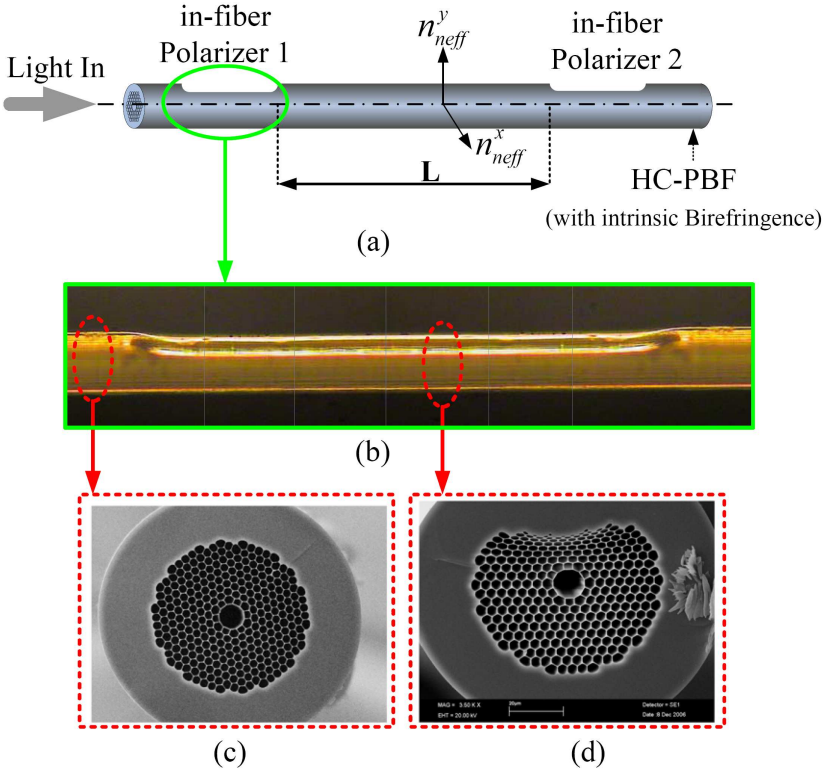

Fig.1 (a) Schematic of an in-fiber PMI, (b) Side view of an in-fiber polarizer formed by CO_2 laser heating the HC-PBF, (c) SEM micrograph of the original HC-1550-02 PBF, (d) Cross-sectional view of the CO_2 laser heated section.

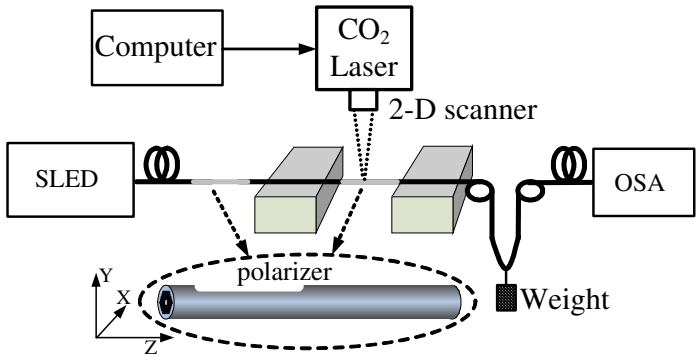

Fig.2 Experimental setup for PMI fabrication

An in-fiber HC-PBF PMI can be fabricated by a two-step process: polarizer 1 on the left as shown in Fig.1(a) is firstly fabricated by following a procedure as described in [16]; polarizer 2 is then fabricated with the same CO2 laser setup but with a different on-line spectrum monitoring system as shown in Fig.2. Instead of monitoring the evolution of polarization-dependent loss (PDL) as in [16], the wavelength-domain interference fringes are monitored during the PMI fabrication process by use of an optical spectrum analyzer (OSA, Aglient 86140B) in combination with a broadband SLED light source. Fig.3 shows an example of recorded transmission spectrum for a PMI with L=531mm, clearly showing the wavelength domain fringes of the PMI.

#112835 - $15.00 USD Received 15 Jun 2009; revised 11 Jul 2009; accepted 12 Jul 2009; published 17 Jul 2009

As illustrated in Fig.3, the contrast of interference fringes grows with the number of repeated CO_2-laser-scanning cycles. The scanning cycle is a parameter defined in [16, 21] and it refers to a complete scanning process of the CO_2 laser across a section of HC-PBF (the length of the CO_2 laser treated region as shown in Fig. 1(b). Repeated scanning across the same section of fiber increases the degree of air-hole collapse and improves the extinction ratio of the polarizer being fabricated. There are fringes with contrast around 0.8dB even before the second polarizer is being fabricated, indicating that there are residual polarization mode coupling or mixing occurring after the first polarizer. After 15 scanning cycles, the fringe contrast increased to above 8 dB over the wavelength range from 1550 to 1650 nm. After 40 scanning cycles, the fringe contrast is about 20 dB or more for wavelength beyond 1550nm.

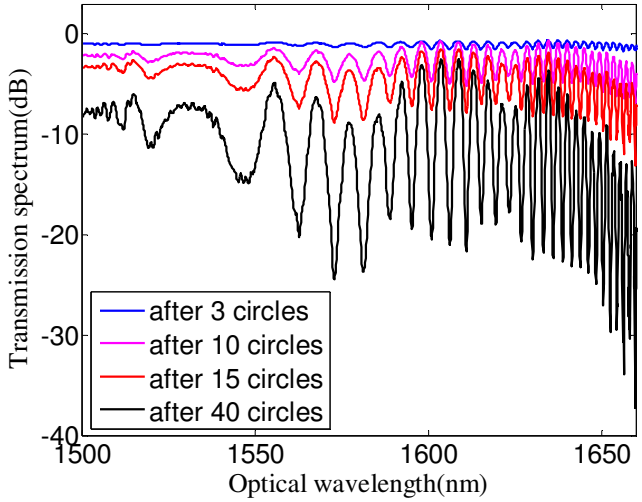

Fig.3 Evolution of wavelength domain fringes during PMI fabrication process. The device length of the PMI is 531mm and the resolution of the OSA is 0.1nm.

3. Measurement of group birefringence of HC-PBF

The wavelength domain fringes as shown in Fig.3 can be used to determine group birefringence of the HC-PBF as function of wavelength [22-24]. It's well known that the wavelength spacing $\Delta\lambda$ between two adjacent fringe peaks or dips may be related, to a first order approximation, to fiber group birefringence B_g by

$$\Delta\lambda \approx \frac{\lambda^2}{B_g L}. \tag{2}$$

In fact, the relationship between absolute value of B_g and optical wavelength λ, may be calculated directly from Fig.3 by using Short-Time Fourier Transform [25]. The results are shown in Fig.4(a) in which the highlighted ridge gives the relationship between $|B_g(\lambda)|$ and λ. For comparison, the dispersion relationships obtained from the Short-Time Fourier Transform and deduced from Differential Group Delay (DGD) measurement with the Agilent 81910a All Parameter Analyzer are both shown in Fig.4(b). The two curves agree well with each other except for wavelength below 1540nm. The discrepancy may be explained as follows: as shown in Fig.3, the oscillatory fringes from 1500 to 1540nm are highly irregular, and the fringe oscillation from 1520 to 1540nm is obviously much slower and this causes the number of fringes over the wavelength window, which was used for our Fourier Transform calculation, much less than one, and hence results in larger calculation error. The accuracy is

#112835 - $15.00 USD Received 15 Jun 2009; revised 11 Jul 2009; accepted 12 Jul 2009; published 17 Jul 2009

expected to improve if the PMI has a longer length, which gives more number of fingers over the wavelength window, is used. As shown in inset of Fig.4(b), the group birefringence in this shorter wavelength range have a minimum indeed, which is agree well with the previous report[19]. As reported previously in [24], the phase birefringence of the PBF may be very low and go through the zero at the shorter wavelength edge of bandgap, and this would cause self-coupling between two polarization modes and result in error or even invalidate the present method for group birefringence. Nevertheless, the good agreement in the longer wavelength side confirms that the PMI technique can be used for group birefringence or DGD measurement of HC-PBFs. The experimental results also verify that HC-1550-2 PBF has a considerable amount of residual group birefringence. The results also further verify that the fringes shown in Fig.3 are the result of interference between the two polarization states of the fundamental mode.

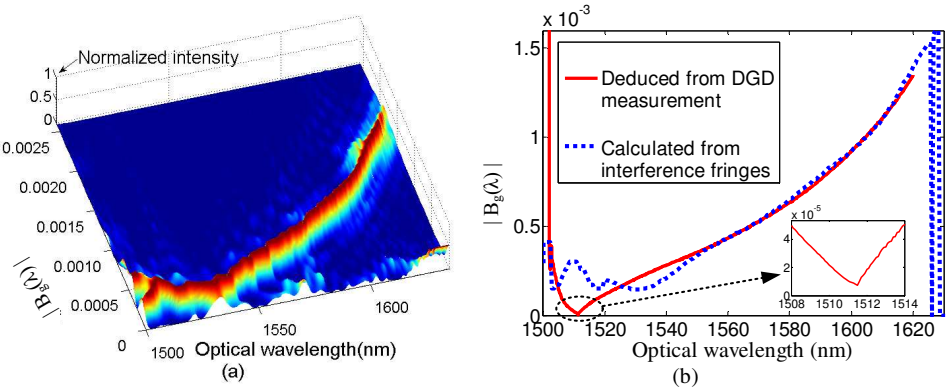

Fig.4 (a) The result obtained from the Short-Time Fourier Transform of Fig.3. (b) $|B_g(\lambda)|$ - λ relationships deduced from Differential Group Delay measurement and from transmission spectrum of PMI.

4. Response of PMI to strain, temperature, and twist

The responses of the PMI to strain, temperature and twist are experimentally studied and the results are shown in Figs.5-10. In the temperature measurement, the transmission spectrum of PMI is monitored when temperature surrounding the HC-PBF is varied from 20 to 100℃ by use of a digitally controlled oven. The comb-like spectrum red-shifts with increasing temperature is shown in Fig.5(a) and the relationship between the dip wavelength around 1624nm and temperature is shown in Fig.5(b), corresponding to a temperature coefficient of ~ 5pm/℃ for a 230mm-length PMI. It should be mentioned that the temperature sensitivity is inversely proportional to device length and, for a PMI with 50mm length, the sensitivity is ~ 0.86pm/℃. This value is ~1000 times smaller than the sagnac interferometer with polarization maintaining side-hole fiber [26], ~100 times lower than the in-fiber modal interferometer based on conventional SMF [10, 12, 27, 28] , ~ 10 times smaller than a typical fiber Bragg grating (FBG) sensor [5] and in-fiber Mach-Zehnder interferometer based on a pair of long-period gratings on photonic crystal fibers[14], and even lower than sophisticated sensor structures reported in [29] for temperature insensitivity. The temperature responses of the dips at three different wavelengths of the 230mm-length PMI are shown in Fig.6(a), while the relative wavelength shifts of the dips with temperature are shown in Fig.6(b). The temperature coefficient of the dip at the 1627.5nm is ~6.2pm/℃, almost twice that of the dip at the 1602.1nm. From the Fig.6(b), it can be found that the temperature sensitivity of different dips is obviously not the same and the dip at longer wavelength is more sensitive to temperature change than those at shorter wavelengths.

#112835 - $15.00 USD Received 15 Jun 2009; revised 11 Jul 2009; accepted 12 Jul 2009; published 17 Jul 2009

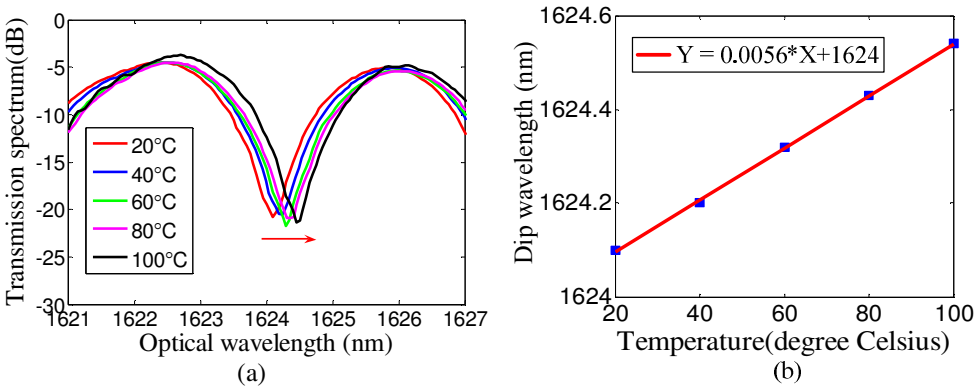

Fig5. (a) Shift of fringe around 1624nm with temperature. (b) Linear fit showing the relationship between the dip wavelength and temperature. The device length of the PMI is 230mm.

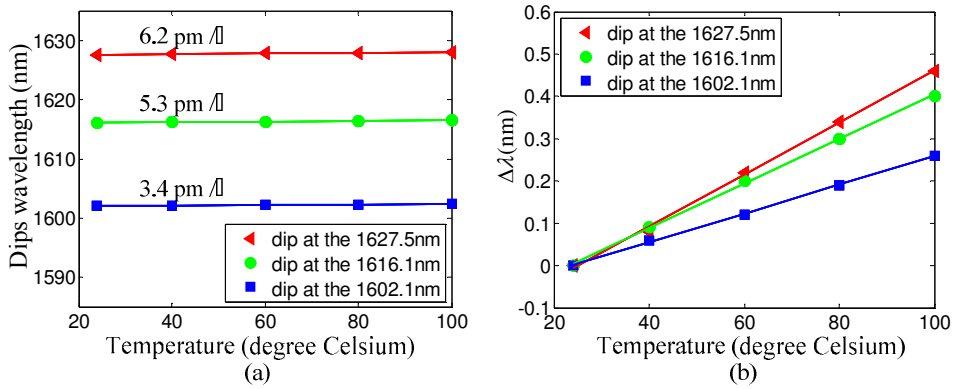

Fig. 6 (a) Temperature responses of three different dips; (b) Relative shift of dip wavelength with temperature. The PMI is the same as that in Fig.5.

The response of the PMI to longitudinal strain is investigated by monitoring the shifts of comb-like peaks or dips by use of an OSA. Contrary to the temperature response, the interference dips move toward shorter wavelength (blue-shift) as longitudinal strain increases. Fig.7(a) shows the shift of the fringe dip around 1626.9nm for a PMI with device length of 531mm. The dip wavelength decreases linearly with applied strain with a coefficient of about 0.6pm/με, as shown in Fig. 7(b). This value is comparable and slightly smaller than FBG sensors [5] and ~10 times smaller than other in-fiber photonic crystal fiber interferometric devices [14] and Sagnac interferometer based on polarization maintaining fiber [26]. For comparison, the strain responses of the three dips at 1630.1nm, 1626.9nm and 1623.4nm are shown in Fig.8. Different fringes have slightly different sensitivity to longitudinal stain, and the dips at shorter wavelengths generally have slightly higher strain sensitivity. This phenomena is opposite to that of the device reported in [26], in which the peak at longer wavelength is more sensitive to strain.

#112835 - $15.00 USD Received 15 Jun 2009; revised 11 Jul 2009; accepted 12 Jul 2009; published 17 Jul 2009

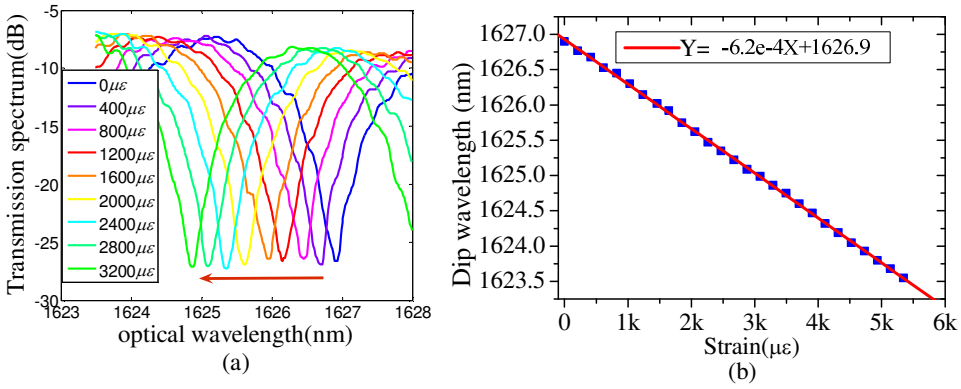

Fig. 7 (a) Shift of fringe around 1626nm with longitudinal strain; (b) Linear fit showing the relationship between the dip wavelength and strain. The device length of the PMI is 531mm

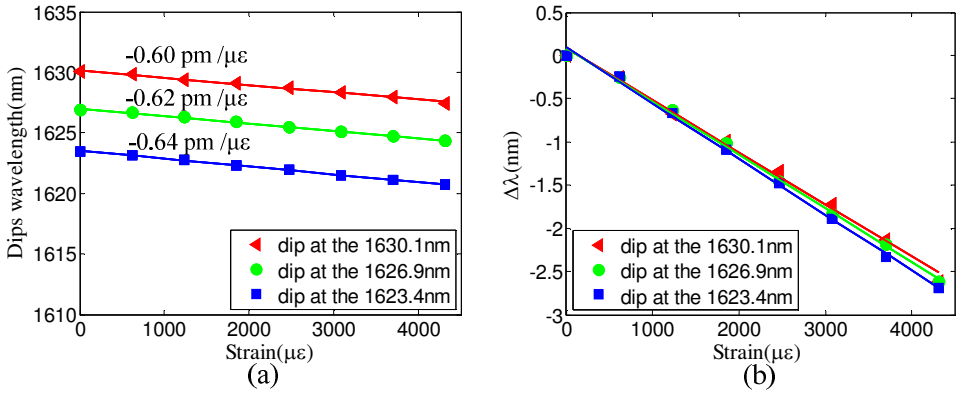

Fig. 8 (a) Strain responses of three different dips at different wavelengths; (b) Relative shift of dip wavelengths with strain. The PMI is the same as that in Fig.7.

One of the unique features of the in-fiber PMI is its response to torsion. Fig.9(a) shows the experimental setup we used for torsion measurement. During experiment, one end of the PMI (the first polarizer) is fixed to a stationary stage, and the other end (the second polarizer) is fixed to the center of a rotatable disc that can be turned to apply twist to the PMI. An 8g mass is attached to the fiber to keep the device straight. A SLED source and OSA are used to measure the transmission spectrum as the PMI is twisted. The device length of the PMI is 147mm. Firstly, the PMI is twisted clockwise by a total angle of 135℃, corresponding to a twist rate of ~16 rad/m. The PMI is then loosened gradually step by step for more measurement points to be taken. The same procedure is repeated anticlockwise. As shown in Fig. 9(b), the dip wavelength around 1628nm changes linearly with the applied twist rate in the region of ±16rad/m. The dip wavelength shifts towards shorter wavelength as the PMI is twisted clockwise, whereas it shiftes toward longer wavelengths as the PMI is twisted anticlockwise. The twist sensitivity is ~70 pm/(rad/m) with good repeatability. This value is bigger than the long-period fiber gratings induced by CO_2 laser pulses [30], ~10 times smaller than the corrugated long-period fiber gratings [31], and ~100 times smaller than the Sagnac interferometer based on polarization maintaining fiber [26]. Further more, the determinations of twist direction were not discussed in [26, 31]. In Fig. 10, the responses of four dips at different wavelengths to twist rate are compared. From Fig.10 (b), it is obvious that the dips at shorter wavelengths have higher sensitivity to twist rate. The sensitivity of the dip at the

#112835 - $15.00 USD Received 15 Jun 2009; revised 11 Jul 2009; accepted 12 Jul 2009; published 17 Jul 2009

1617.4nm, is ~110pm/(rad/m), approximately 2.5 times larger than that of the dip at 1646.2nm.

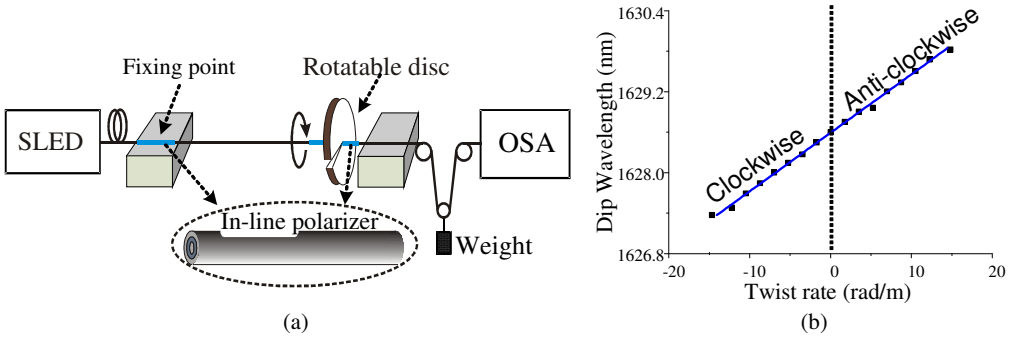

Fig. 9(a) Experimental setup for testing the torsion characteristics of the PMI (b) Dip wavelength against twist rate applied. The device length of the PMI is 147mm

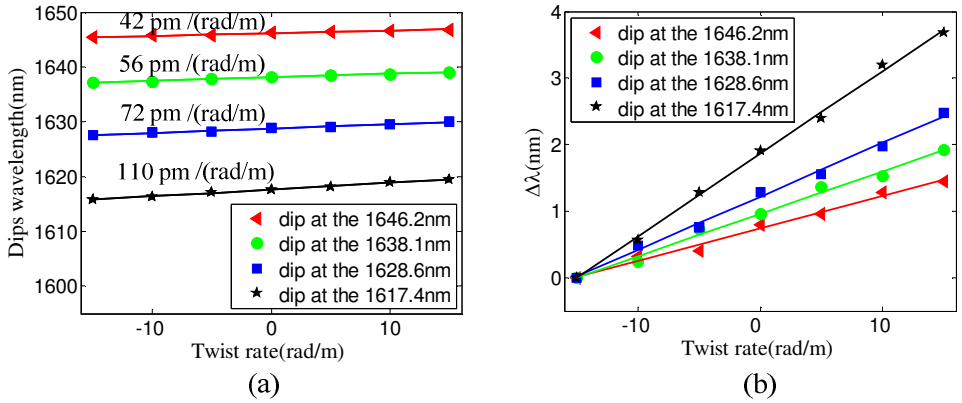

Fig. 10 (a) Responses of different dips to twist rate. (b) Relative shift of dip wavelengths with twist rate. The PMI is the same as in Fig. 9.

5. Conclusion

The interference between the two orthogonal polarization components of fundamental mode in a HC-PBF is realized by fabricating two in-fiber polarizers along a single PBF by use of a pulsed CO_2 laser. The response of such made in-fiber polarimeters to strain, temperature and twist is experimentally studied. The interference fringe dip wavelength is found to shifts toward short wavelength with increasing longitudinal strain and has a strain sensitivity of about 0.6pm/με. The dip wavelength has much smaller temperature sensitivity (about 0.86pm/℃ for a polarimeter of 50mm in length) compared with those previous in-fiber modal interferometers, indicating the device may be used as temperature insensitive strain sensors and comb-filters. A particular application of the PMI is for torsion measurement in which the direction and rate of the applied twist may be determined at the same time. Because of the very low loss of the fundamental mode as compared with cladding modes in index guiding fibers, the in-fiber PMI can be design to have either short or long device length, and hence allow for wider range of applications.

Acknowledgement

The research work was supported by the Research Grant Council of the Hong Kong SAR Government through a GRF grant PolyU5182/07E, and NSF of China though grant no: 60629401.

#112835 - $15.00 USD Received 15 Jun 2009; revised 11 Jul 2009; accepted 12 Jul 2009; published 17 Jul 2009